
Measurement Technique for Characterization of Rapidly Time- and Frequency-Varying Electronic Devices

The conventional method for measuring the transfer function of an electronic device uses Fourier transform theory and convolutions and is, therefore, limited to either time-invariant or frequency-invariant devices. The measurement technique presented here enables the complete characterization of electronic devices having any dynamic temporal and spectral frequency response. A technique presented earlier¹ applied the windowing of signals in the time and frequency domains (called time-frequency distributions) to characterize photoconductive switches that vary in time *and* frequency; however, windowing requires a slowly varying envelope approximation, which limits the allowed rate of temporal and spectral variations. The more general technique allows us to measure the frequency response of the optoelectronic (photoconductive) microwave switches on OMEGA's pulse-shaping system. Unlike microwave diode switches, photoconductive switches do not have a constant conductive on-state, but rather decay monotonically to the off-state after the illumination ceases. A complete linear model for such a device must incorporate both filtering and modulation into a general time-varying filter (or equivalently, band-limited modulator). Any microwave or millimeter-wave device whose properties vary rapidly requires the application of this technique for complete characterization, including elements that depend on charge-carrier dynamics such as photoconductive attenuators, phase shifters, and directional couplers.

The general concept of a linear, time-varying filter is well established in the signal-processing,^{2,3} communication,⁴ and automatic control⁵ fields. In the microwave-device field, however, the linear variations of filter properties are typically due to slowly varying mechanisms (e.g., mechanical) or are generated by rapid transitions between steady-state regimes (e.g., microwave diode switches); therefore, a form of windowing is usually adequate for characterization. The analysis presented here introduces a characterization technique analogous to (and a superset of) a form of input–output relationships called the scattering or S parameters, which can be applied to devices that can be considered linear filters with rapid modulation of amplitude and/or phase (e.g., photoconductive switches). In

the next section we briefly discuss the complementary relationship between linear filters and linear modulators. From this conceptual viewpoint, we derive an extension of the filter and modulator characterization functions $S(\omega)$ and $k(t)$ to a general linear device characterization or system function $\tilde{S}(\omega, t)$. Based on the limitations of conventional S -parameter analysis in the **Mathematical Formulation** section, we present some important properties of the \tilde{S} parameter and explain conditions under which this form of analysis can be implemented. In the **Analytical Example** section we apply our \tilde{S} -parameter concept to device analysis by considering a simplified lumped-element example, deriving the \tilde{S} parameters from the theory and directly from the differential equations, and demonstrate the limitations of windowing. Photoconductive switches used on OMEGA pulse shaping have been optimized through the application of the \tilde{S} -parameter technique; these results will be presented in a separate article.

Background

Conventional microwave device characterization depends on shift-invariant device models for characterization, taking advantage of the property that a convolution in one domain Fourier transforms to multiplication in the other. In Table 78.VI the canonical input–output relationships of the two ideal shift-invariant microwave devices are presented to emphasize their complementary nature. All dependent variables are complex, $a(\omega)$ and $b(\omega)$ are the Fourier transforms of the respective input and output temporal power waves $A(t)$ and $B(t)$, $S(\omega)$ and $h(t)$ are the scattering parameter and its Fourier transform (the impulse response), k and K are the modulation parameter and its Fourier transform, and the subscripts refer to the microwave input–output ports of the device. The linear-frequency-invariant (LFI) model of a modulator is valid when narrow-band input signals (relative to the modulator bandwidth) are applied, and the linear-time-invariant (LTI) filter model is valid when the device's temporal variations are longer than the signal duration. Note that here and throughout this article, for the convenience of using notation familiar in measurement practice, we use ω for $j\omega$ and draw no distinction between real and analytic time-series signals.

Table 78.VI: A comparison of the transfer functions of shift-invariant devices: an ideal, linear-time-invariant (LTI) filter and frequency-invariant (LFI) modulator.

	Time Domain	Frequency Domain
Time-invariant filter	$B_i(t) = \int_{-\infty}^{\infty} h_{ij}(t - \tau) A_j(\tau) d\tau$	$b_i(\omega) = S_{ij}(\omega) \cdot a_j(\omega)$
Frequency-invariant modulator	$B_i(t) = k_{ij}(t) \cdot A_j(t)$	$b_i(\omega) = \int_{-\infty}^{\infty} K_{ij}(\omega - \xi) \cdot a_j(\xi) d\xi$

The analysis based on the equations in Table 78.VI cannot be applied to a device that is neither time invariant nor frequency invariant. As Fig. 78.47 indicates, a time-varying filter will have different impulse responses at different times [(b) and (c)], or equivalently a modulator with finite frequency response will modulate different frequencies differently [(d) and (e)]; so neither model in Table 78.VI is adequate for complete characterization. If the device can be held constant in one domain independently of the other, or if the variations are slow relative to the signal applied, conventional analysis can be applied by using some form of windowing; inaccuracies will depend on how strongly the LTI or LFI assumptions are violated. If the filtering and modulating aspects of this general linear device cannot be controlled independently (i.e., cannot be made separable) and the variations in time and frequency are rapid, characterization of the device under test (DUT) using either $k(t)$ modulator functions or $S(\omega)$ filter parameters cannot account for complete device behavior. Since conventional methods of linear microwave circuit characterization (e.g., spectrum and network analyzers) are based on the application of Fourier transforms and the convolution integral, their use can lead to incorrect or even misleading characterization results.

Motivated by these limitations, we combine the separate (but complementary) one-dimensional (1-D) LTI and LFI transfer functions to a single two-dimensional (2-D) transfer (or system) function, calling it $\tilde{S}(\omega, t)$ to emphasize its similarity to conventional $S(\omega)$ parameters. For illustration, a conceptual example of the amplitude of an exponentially decaying, low-pass filter is shown in Fig. 78.47(f). This 2-D parameter can be more difficult to measure than a conventional device's $S(\omega)$ parameters; however, the measurement process can be simplified by taking advantage of the 2-D nature of \tilde{S} and using methods that are not applicable 1-D functions. For example, the theory of generalized projections as used in 2-D phase retrieval allows us to reconstruct the full, vector (complex) 2-D transfer function \tilde{S} by measuring only the magnitude $|\tilde{S}|$. Although generalized projections are restricted to

functions that are zero outside some finite temporal and spectral window (i.e., that have known, compact support along both axes⁶), in practice the transfer functions of microwave devices satisfy this criteria.

$\tilde{S}(\omega, t)$ can be applied to device characterization in the *frequency domain* or the *time domain*. Conceptually, in the frequency-domain approach a single-frequency wave can be applied to the DUT for the time duration of interest, and then the temporal evolution of the resulting output signal's amplitude and phase can be recorded. Next, to separate the device's effect on signal amplitude and phase, the same input wave is applied, phase shifted by $\pi/4$, over the same time duration relative to the trigger, and again the temporal evolution of amplitude and phase is recorded (i.e., this is equivalent to measuring the analytic signal). Finally, by reapplying signals at different frequencies, a map of $\tilde{S}(\omega, t)$ can be generated for the DUT by constructing successive time slices at each frequency. Alternatively, in the time-domain approach a series of impulse functions can be applied at appropriate time intervals over the period of interest, and the impulse response corresponding to each input can be recorded. Although these descriptions are intuitively appealing, it may not be readily apparent how to extract an input–output relationship such as $\tilde{S}(\omega, t)$ from the measured signals, apply it to the calculation of output signals given an arbitrary input signal properly, and avoid the effects of windowing. The following analysis will clarify the technique and the method of calculation.

Mathematical Formulation

To derive a combined system function $\tilde{S}(\omega, t)$ that is capable of characterizing the input–output relationships of devices that are neither exclusively modulators nor filters and is easily determined by measuring the incident and emerging signals, we must revisit some of the assumptions used in microwave circuit/network analysis and synthesis. To emphasize the utility of our more generalized transfer function, we will frame our discussion in terms of filters and S -parameter characterization; however, the system function $\tilde{S}(\omega, t)$ sub-

sumes both LFI and LTI devices as special cases, so it is equally applicable to modulators. The route taken is motivated by the observation that, in the equations for filters and modulators presented in the previous section, the roles of time and

frequency are complementary, i.e., the 1-D characterization functions are along orthogonal axes in the complex plane. From this comes the realization that a more general, 2-D characterization is possible by considering and measuring the device's response on the entire plane.

A convenient place to begin the derivation is with the time-domain differential equation describing a linear lumped-element device with time-variable coefficients:

$$\alpha_0(t) \frac{d^n}{dt^n} B(t) + \alpha_1(t) \frac{d^{n-1}}{dt^{n-1}} B(t) + \dots + \alpha_n(t) B(t) = \mathcal{L}(p, t) B(t) = A(t), \quad (1)$$

where the coefficients α are determined by the (time-varying) dependencies between the ports (e.g., the lumped-element models of resistance, capacitance, and inductance). The signals $A(t)$ and $B(t)$ are defined as in Table 78.VI, and we've used the operator notation

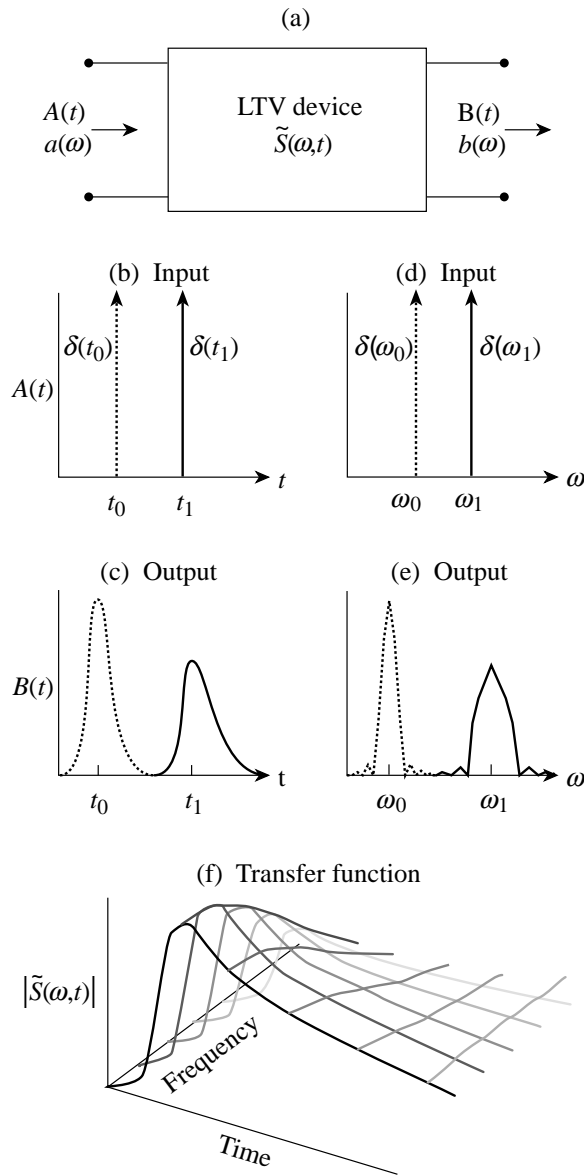
$$\mathcal{L}(p) = \alpha_0(t)p^n + \alpha_1(t)p^{n-1} + \dots + \alpha_n(t),$$

where p is the differential operator d/dt .⁷ Note that although the following derivation is for a device with a finite number of (time-varying) poles and zeros, $\tilde{S}(\omega, t)$, like $S(\omega)$, is equally applicable to distributed-element devices.

For the ideal filter model there is no time variation in the coefficients and Eq. (1) simplifies to

$$\mathcal{L}_{ij}(p) B_1(t) = A_j(t). \quad (2)$$

Assuming complex exponentials for the basis functions (so that the differential operator becomes ω) and converting to S -parameter notation $S_{ij}^{-1}(\omega) = \mathcal{L}_{ji}(p)$, we derive the frequency-domain filter transfer function of Table 78.VI, and the process is analogous for the ideal modulator model. The use of complex exponential basis functions as solutions in the transform integral leads to the formalism of Fourier transforms. Fourier transforms are useful for microwave-device characterization because they transform between a system of differential equations and a system of algebraic equations; that is to say they are *compatible* integral transform operators.⁸ Non-compatible transforms do not result in simple convolution or multiplicative relationships between input and output ports.



Z2404

Figure 78.47 (a) Signal flow for a general linear-time- and frequency-varying device. Time variation is shown schematically by (b) identical impulses applied at different times, which result in (c) different impulse responses. Frequency variation is shown by (d) two different input sine waves and (e) differences in their modulated output spectral functions. (f) A representative sketch of the magnitude of the resulting transfer function $\tilde{S}(\omega, t)$ shows exponential time decay and low-pass filtering, such as might occur with OMEGA's photoconductive switches.

In contrast to ideal modulators and filters, for a general device a compatible integral transform operator depends on the functional form of the variable coefficients in Eq. (1). This means that the basis functions are not, in general, $e^{\pm j\omega t}$ but rather are dependent on the particular form of modulation and frequency response. To keep the analysis independent of the details of the modulation and frequency response, we will choose a noncompatible transform such that we are able to continue to use $e^{\pm j\omega t}$ basis functions; this is the key point of this characterization technique. Some important implications of this choice will be mentioned as we derive properties of the system function resulting from this choice of integral transform.

A definition of the general linear device system function is

$$\tilde{S}_{ij}(\omega, t) = \left. \frac{B_i(t)}{A_j(t)} \right|_{A_j(t)=e^{j\omega t}}, \quad (3)$$

which differs from the traditional S -parameter definition in that it is now a function of time as well as frequency. In addition $\tilde{S}_{ij}^{-1}(\omega, t) = \mathcal{L}_{ji}(p, t)$, where the differential operator p transforms to ω by differentiation of $e^{j\omega t}$; therefore, $B_i(t) = \tilde{S}_{ij}(\omega, t)e^{j\omega t}$ is the output of the device for an input $A_j(t) = e^{j\omega t}$, given that the device is in a known state at every time $t \geq t_0$ (i.e., the variable coefficients evolve deterministically from time $t = t_0$). Due to the linearity of the device, by superposition the output $B_i(t)$ is defined in terms of $A_j(\tau)$ according to

$$B_i(t) = \int_0^t \tilde{h}_{ij}(\tau, t) A_j(\tau) d\tau. \quad (4)$$

Equation (4), where the impulse response function $\tilde{h}_{ij}(\tau, t)$ is now the more general Green's function, is a generalization of the time-invariant convolution in Table 78.VI in that the impulse response no longer depends only on the *age* from impulse time τ to observation t . Substituting Eq. (4) into Eq. (3) results in a transform relationship between the system function $\tilde{S}(\omega, t)$ and the new generalized impulse response $\tilde{h}_{ij}(\tau, t)$:

$$\tilde{S}_{ij}(\omega, t) = \int_{-\infty}^{\infty} \tilde{h}_{ij}(\tau, t) e^{-j\omega(t-\tau)} d\tau. \quad (5)$$

Notice that (a) $\tilde{S}(\omega, t)$ and $\tilde{h}_{ij}(\tau, t)$ are related by a Fourier transform of the first axis and (b) two other system function definitions result from transforming each of these in the second

variable. We can visualize the fundamental difference between (a) these 2-D system functions that are characterizations of time- and frequency-varying devices and (b) system functions that are determined from windowed signals: the feature size of a 2-D system function (the mountains and valleys of the surface plot) along one axis is independent of the other axis, whereas (due to the uncertainty principle) the features of a system function along each axis generated by windowing are related to each other by the Fourier transform. In other words, a narrow windowing of a signal in time (necessary to prevent averaging of the system's time fluctuations) implies a widening of the spectral window (which forces averaging over spectral fluctuations), and vice versa. In the next section we show this difference in more detail by applying ambiguity functions and time-frequency distributions.⁹⁻¹²

From Eq. (4) we get a relationship between input and output by replacing $A_j(t)$ with its transform $\int a_j(\omega)e^{j\omega t} d\omega$, inverting the order of integration, and substituting from Eq. (5):

$$B_i(t) = \mathcal{F}^{-1} \left\{ \tilde{S}_{ij}(\omega, t) a_j(\omega) \right\}, \quad (6)$$

where the differential transform operator $\mathcal{F}^{-1} \{ \}$ is essentially the inverse Fourier transform but with the variable t held as a constant parameter. Equation (6) is similar to the frequency-domain filter relation in Table 78.VI in that the signal $B(t)$ is the transform of the product of the S (or in this case \tilde{S}) parameter and the input spectral function. Unlike conventional Fourier transforms, however, Eq. (4) is not a convolution, and the argument inside the brackets of Eq. (6) is not the product of two 1-D functions; therefore, it is not possible to relate the output signal algebraically to the input signal:

$$b_i(\omega) \neq \tilde{S}_{ij}(\omega, t) a_j(\omega). \quad (7)$$

Importantly, the complete function $\tilde{S}(\omega, t)$ cannot be found by taking a quotient $b(\omega)/a(\omega)$ as it can be when finding $S(\omega)$ for LTI devices. For network synthesis, where a model (or equivalently a differential equation) must be synthesized from a given (measured) $\tilde{S}(\omega, t)$ or $G(\tau, t)$, this consequence of non-compatible transforms has no major implications and in fact choosing the noncompatible Fourier transform allows one to use standard transform tables, making the synthesis easier. For network analysis, however, where the output $B(t)$ is found in terms of $A(\tau)$, the significance of Eq. (7) is that only simple linear time- and frequency-varying device models (having first- or second-order differential equations) can be used since

signal flow graphs and the combination of series and parallel devices are no longer algebraic or even analytic, as explained in the next paragraph.

For network analysis using $\tilde{S}(\omega, t)$ of microwave systems with time- and frequency-varying elements, the network must be broken down into block diagrams where the linear time- and frequency-varying element is isolated from the rest of the (conventionally analyzed) LFI or LTI components. The block diagram approach then requires operational methods that combine the general linear element with other components, both in cascade and parallel, to determine the overall system function. For two linear devices in parallel this is trivial; they can be combined by adding their impulse response functions, or equivalently adding their transfer functions.¹³ For two devices in series, however, the combination depends on shift invariance: the overall transfer function of two LTI devices in series is accomplished by multiplying the individual transfer functions together, or equivalently convolving their impulse responses. For two LFI devices in series the transfer (modulation) functions are multiplied, while the spectral transform of the modulation is convolved.

To derive the transfer function of two general linear devices in series, we begin with the repeated operation of the transfer function (in operational form):

$$\tilde{S}(p, t)[a(\omega)] = \tilde{S}_b(p, t)\{\tilde{S}_a(p, t)[a(\omega)]\}, \quad (8)$$

where $\tilde{S}_a(p, t)$ and $\tilde{S}_b(p, t)$ are the transfer functions for the first and second device, respectively, and $a(\omega) = e^{j\omega t}$ is assumed. Since $\tilde{S}_b(p, t)$ will operate on both $\tilde{S}_a(p, t)$ [now $\tilde{S}_a(\omega, t)$ due to the form of its operand] and $A(t)$, we get

$$\begin{aligned} \tilde{S}e^{j\omega t} &= \tilde{S}_b\left(e^{j\omega t} \frac{\partial}{\partial t} \tilde{S}_a + \tilde{S}_a \frac{\partial}{\partial t} e^{j\omega t}\right) \\ &= \tilde{S}_b \frac{\partial}{\partial t} \tilde{S}_a e^{j\omega t} + \tilde{S}_b \omega \tilde{S}_a e^{j\omega t} \end{aligned} \quad (9)$$

and therefore

$$\tilde{S}(p, t)a(\omega) = \tilde{S}_b(p + \omega, t)\left[\tilde{S}_a(p, t)a(\omega)\right]. \quad (10)$$

Analytical Example

To demonstrate the application of \tilde{S} to microwave-device characterization, a representative lumped-element device will be solved analytically. The device shown in Fig. 78.48 is a single-pole, low-pass RC filter with a sinusoidally varying capacitive element $C(t) = C_0 + C_m \sin(\omega_m t)$, where suitable values of the variables are chosen for convenience: $C_0 = 1$ pF is the steady-state capacitance, $C_m/C_0 = 0.2$ is the modulation depth, and $\omega_m = 2.3$ Grad/s is the modulation rate.

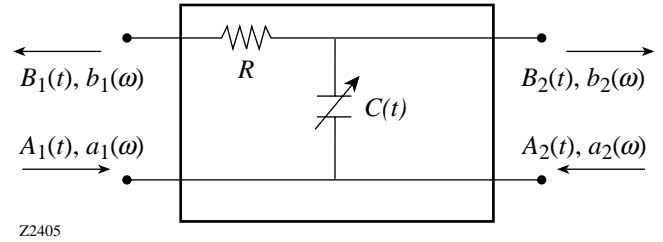


Figure 78.48

An example linear device with a time-varying capacitance and therefore time-varying pole location (bandwidth). This device is linear but cannot be modeled as only a filter or a modulator.

The differential equation for this device, written in the form of Eq. (1), is

$$\begin{aligned} \left[\frac{1}{2}C(t)(R + Z_0)\right] \frac{d}{dt} B(t) \\ + \left[1 + \frac{1}{2}R/Z_0 + \frac{1}{2}(R + Z_0) \frac{d}{dt} C(t)\right] B(t) = A(t). \end{aligned} \quad (11)$$

From S -parameter analysis the S_{21} for a conventional LTI filter like Fig. 78.48 is

$$S_{21}(\omega) = \frac{2Z_0}{2Z_0 + R + j\omega CZ_0(R + Z_0)}. \quad (12)$$

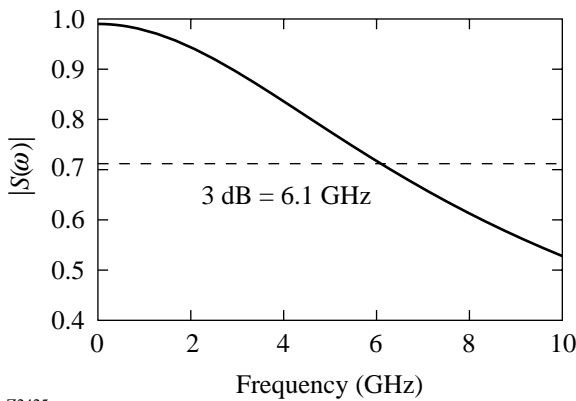
Applying Eq. (10) to the cascade elements of the resistor and shunt capacitor, we get

$$\tilde{S}_{21}(\omega, t) = \frac{2Z_0}{2Z_0 + R + (p + j\omega)CZ_0 \cdot (R + Z_0)}, \quad (13)$$

which could also be found by directly solving the differential equation in Eq. (11). The $|S_{21}(\omega)|$ plot for the LTI version of this device (where the time invariant $C = C_0$) is shown in Fig. 78.49, and $|\tilde{S}_{21}(\omega, t)|$ is shown in the elevation plot of

Fig. 78.50 for one cycle of modulation. Observe in both figures the low-pass attenuation along the frequency axis and for Fig. 78.50 the sinusoidal modulation of the frequency response along the temporal axis.

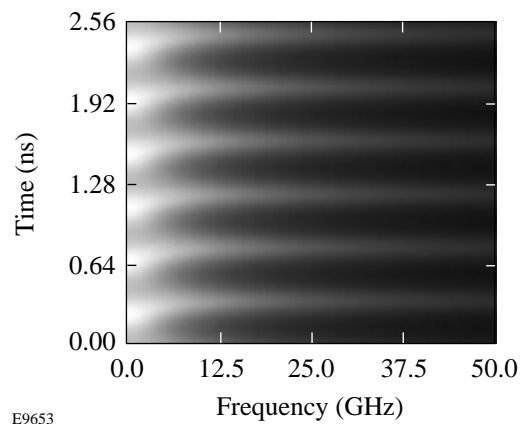
To further illustrate the properties of the time-varying system function we show a surface-density plot of $|\tilde{S}(\omega, t)|$ (Fig. 78.51) over several cycles of modulation and from dc to 50 GHz. Figure 78.51 will also be used in conjunction with the windowed signal to show the limitations of windowing. An aspect of this \tilde{S} shown clearly here is the skew in the peak of the temporal modulation near the 3-dB point of 6.1 GHz, due to the phase shift in the transmission function that occurs at this frequency.



Z2425

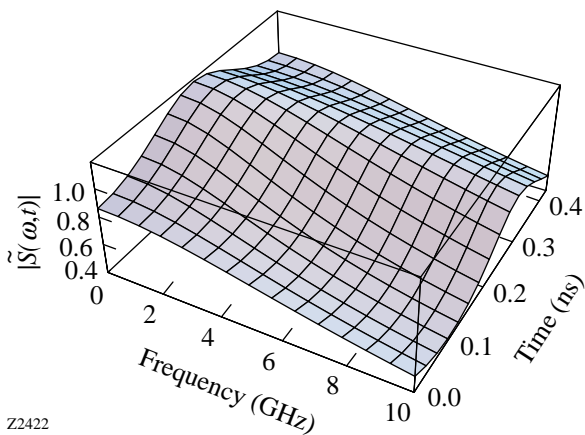
Figure 78.49
Magnitude of the transfer function $|S_{21}(\omega)|$ of a low-pass, single-pole filter that is equivalent to the circuit in Fig. 78.48 but with no time-variation in the capacitance.

Figure 78.52 is a cross section of the transfer function along the time axis, showing the modulating aspect of the device, which is seen to be frequency dependent. The cross sections of $|\tilde{S}|$ along the frequency axis (Fig. 78.53) show the low-pass filter effect of the device and indicate that the shape of the frequency response depends on time. Although stability considerations are outside the scope of this article, both Figs. 78.52 and 78.53 indicate that the instantaneous magnitude can rise momentarily above unity, resulting in a gain in the system over a short time span and finite spectral band. Modulating the capacitance causes a transfer of energy in and out of the system, and with proper terminations it is possible to create an oscillator.



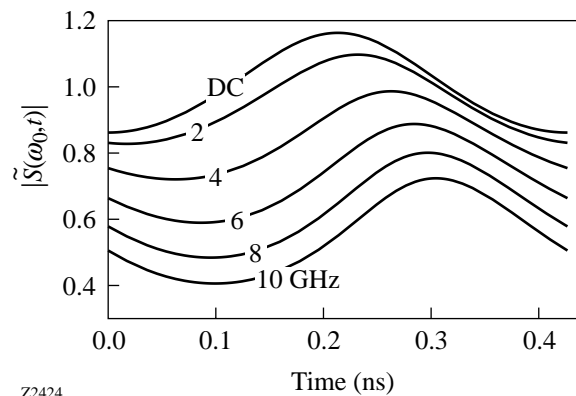
E9653

Figure 78.51
Surface-density plot of $|\tilde{S}(\omega, t)|$ for six cycles of modulation along the time axis and demonstrating low-pass filtering along the frequency axis.



Z2422

Figure 78.50
Magnitude of the transfer function $|\tilde{S}_{21}(\omega, t)|$ of a low-pass, single-pole filter with sinusoidally varying capacitance, plotted over one cycle of modulation in time and over 150% of the bandwidth in frequency.



Z2424

Figure 78.52
A series of cross sections through $|\tilde{S}(\omega, t)|$ along the time axis, showing the change in the magnitude and phase of the modulation for different frequencies.

Using Eqs. (6) and (13) we simulated the propagation of the sum of 5.9- and 19.5-GHz sine waves through the device. The attenuation and dispersion of each spectral component are demonstrated in Fig. 78.54, where the low-pass features are readily apparent in the output signal (solid line) as compared with the input signal (dashed line). The influence of the modulation can best be compared in Fig. 78.55, where the sinusoidal modulation puts discrete sidebands on each spectral component; however, since only magnitude is plotted, the phase shift of the modulation between different frequencies cannot be observed. Since this device not only modulates each frequency differently but also filters the signals, application of network or spectrum analysis would not adequately characterize the device.

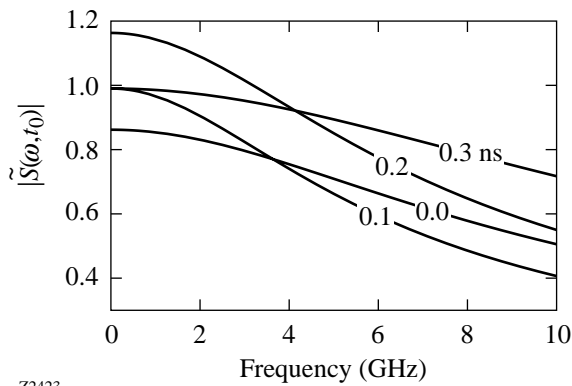


Figure 78.53
A series of cross sections through $|\tilde{S}(\omega, t)|$ along the frequency axis, showing the change in instantaneous bandwidth at different times.

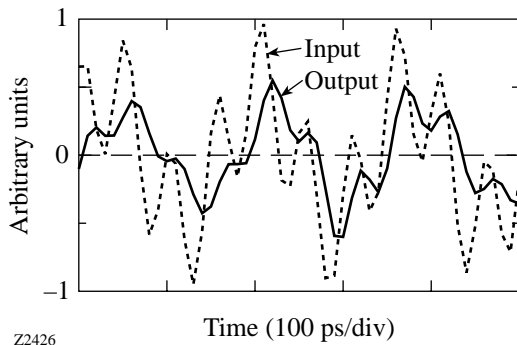


Figure 78.54
Plot of input and output signals showing the DUT's low-pass filtering effect. Dashed line is the input signal; solid line is the output signal.

In the remainder of this section we use windowed signals in an attempt to adequately characterize our time-varying filter with conventional *S*-parameter analysis, and we compare the results to our previous approach. For the windowing we use time–frequency distributions because of their appealing representation, and because they more intuitively demonstrate the fundamental constraint; due to the uncertainty principle, a narrow windowing in time necessarily leads to a broad frequency window. This is seen on a time–frequency representation by the phenomenon of *minimum area*: a surface-density plot of the time–frequency distribution of a signal consists of areas (or regions) where the signal exists at a localized time and frequency, which cannot be smaller than a constant determined by the uncertainty principle. The uncertainty is inherent to windowing in general and not time–frequency distributions in specific, so therefore the choice of specific time–frequency distributions to demonstrate the uncertainty limitations of windowing doesn't detract from the generality of the result.

To demonstrate the limitations of windowing, the particular choice of algorithm to generate a time–frequency representation is a matter of convenience: for this example we will use

$$A(\omega; t) = \int_{-\infty}^{\infty} A(t) \omega e^{-j\omega^2(t-\tau)^2} dt, \quad (14)$$

where $A(\omega; t)$ is the time–frequency distribution of $A(t)$ and a semicolon is used between the joint time–frequency variables to stress the dependence of the axes. This definition has the virtues of showing all the essential features of time–frequency

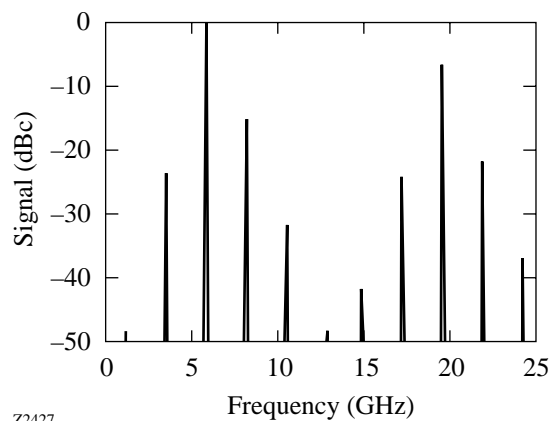


Figure 78.55
Spectral plot of output signal, showing the change in modulation characteristics for different frequencies.

distributions and (due to the use of a Gaussian window) being easily transformable back into the Fourier transform of the signal $a(\omega)$ by integration:

$$a(\omega) = \int_{-\infty}^{\infty} A(\omega; t) dt. \quad (15)$$

Figure 78.56 shows an example windowed signal to be propagated through our system: a 2-GHz sine wave that abruptly transitions after 1.28 ns (with broadband noise) to a 20-GHz sine wave. The smearing of the signal in time (for the low-frequency signal) and frequency (for the high-frequency signals) due to windowing trade-offs (which are ultimately due to the uncertainty relationship) can be easily seen. The use of the FFT to generate the time–frequency distribution (which assumes a continuous, periodic signal) caused leakage to occur across the time boundary (top and bottom) of each spectral component of the signal; for the low-frequency signal, the leakage is significant enough to bridge the span over which it is ostensibly “off.”

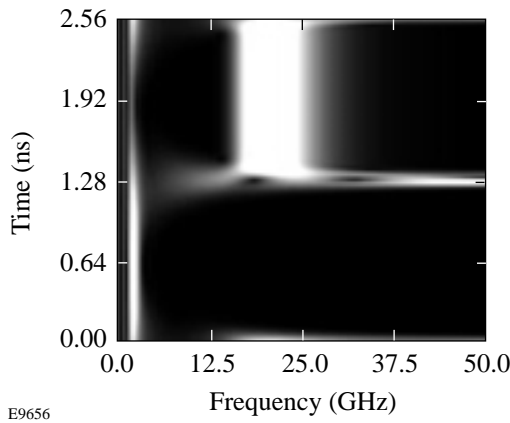


Figure 78.56 Time–frequency representation (ambiguity function) of a 2-GHz sine wave that transitions abruptly to a 20-GHz sine wave with broadband noise at the transition.

By multiplying the input signal $A_1(\omega; t)$ of Fig. 78.56 with the system function $\tilde{S}_{21}(\omega, t)$ of Fig. 78.51 we get the time–frequency distribution of the output signal $B_2(\omega; t)$ (shown in Fig. 78.57). Important features of the resulting output signal, as evidenced in the time–frequency distribution, are the significantly different modulation of each spectral component and the low-pass filtering, which attenuates the high-frequency component. Converting back to the time domain using Eq. (15) and then inverse Fourier transforming, we can com-

pare the resulting output signal with our technique. The windowing technique gives the solid line in Fig. 78.58, while our result is the dashed line. It is evident that although windowing produced acceptable results for the second half of the signal when the modulation was much slower than the signal (i.e., the slowly varying envelope approximation), for the first half of the signal, the modulation was comparable to the signal frequency so the window effectively smeared the modulation

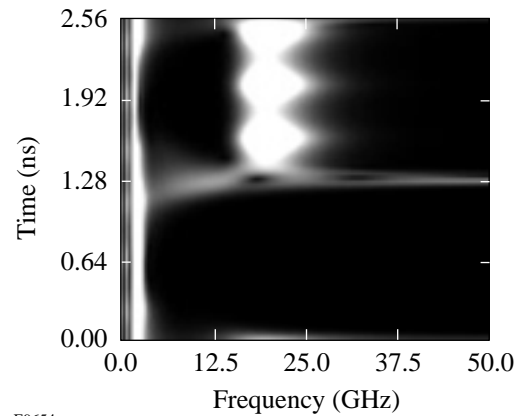


Figure 78.57 Time–frequency representation of the output signal, after multiplication of the input time–frequency distribution with the system function $\tilde{S}(\omega, t)$. The effect of the system function is shown by the attenuation of the broadband noise and the ripple in the two spectral components of the signal.

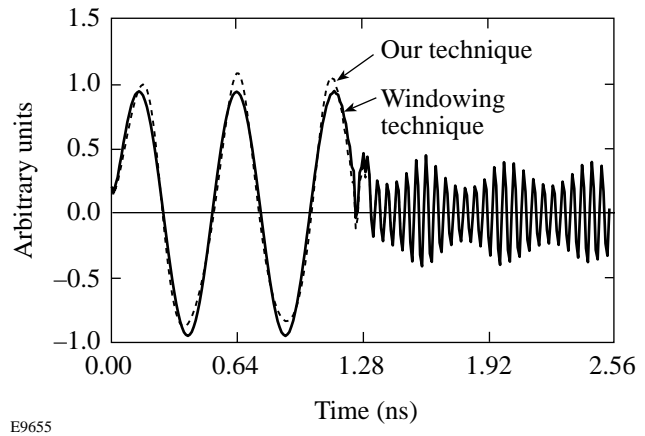


Figure 78.58 Time-domain comparison of output signals using the technique described in this article (dashed) and the windowing method (solid). The windowing appears acceptable for high-frequency signal component where the modulation is gradual, but it washes out the temporal modulation for the low-frequency component.

in time. Choosing a narrower window would not solve the fundamental problem since doing so would necessarily broaden the spectral window, causing increased smearing of the spectral response.

Conclusions

The goal of this work is to completely characterize photoconductive microwave switches regardless of the temporal and spectral variations in their frequency response (transfer function). The unique photoconductive properties of these devices that enable their use in OMEGA's pulse-shaping system also require a characterization technique that accounts for the switch's frequency and time variations simultaneously. The analysis presented in this article provides such a characterization technique and is currently being applied to the switches to optimize their pulse-shaping performance. To characterize such devices, we take advantage of the complementary aspects of LTI and LFI 1-D transfer functions and combine them into a single linear device system function $\tilde{S}(\omega, t)$. This 2-D transfer function allows us to synthesize network models based on measurements of device responses that vary rapidly in frequency as well as time. We discussed several important properties of this new \tilde{S} parameter, showing similarities to conventional S -parameter analysis that preserve most features of the familiar Fourier transform tables. The transfer function of an analytical linear time-varying device was calculated and compared to that of an LTI filter, and the utility of the $\tilde{S}(\omega, t)$ function concept was demonstrated while also showing the limitations of windowing.

ACKNOWLEDGMENT

This work was supported by the U.S. Department of Energy Office of Inertial Confinement Fusion under Cooperative Agreement No. DE-FC03-92SF19460 and the University of Rochester. The support of DOE does not constitute an endorsement by DOE of the views expressed in this article. Kenton Green also acknowledges the support of the Frank Horton Graduate Fellowship Program.

REFERENCES

1. Laboratory for Laser Energetics LLE Review **76**, 225, NTIS document No. DOE/SF/19460-264 (1998). Copies may be obtained from the National Technical Information Service, Springfield, VA 22161.
2. G. W. Wornell, Proc. IEEE **84**, 586 (1996).
3. C. Bor-Sen, C. Yue-Chiech, and H. Der-Feng, IEEE Trans. Signal Process. **46**, 3220 (1998).
4. L. Heung-No and G. J. Pottie, IEEE Trans. Commun. **46**, 1146 (1998).
5. L. M. Silverman, IEEE Trans. Autom. Control **AC-16**, 554 (1971).
6. H. Stark, ed. *Image Recovery: Theory and Application* (Academic Press, Orlando, 1987).
7. G. H. Owyang, *Foundations for Microwave Circuits* (Springer-Verlag, New York, 1989), Chap. 10, pp. 541–606.
8. H. D'Angelo, *Linear Time-Varying Systems: Analysis and Synthesis*, The Allyn and Bacon Series in Electrical Engineering (Allyn and Bacon, Boston, 1970).
9. B. Boashash, Proc. IEEE **80**, 520 (1992).
10. H. N. Kritikos and J. G. Teti, Jr., IEEE Trans. Microw. Theory Tech. **46**, 257 (1998).
11. S. R. Kunasani and C. Nguyenj, IEEE Microw. Guid. Wave Lett. **6**, 1 (1996).
12. H. Ling *et al.*, IEEE Trans. Antennas Propag. **41**, 1147 (1993).
13. W. Kaplan, *Operational Methods for Linear Systems*, Addison-Wesley Series in Mathematics (Addison-Wesley, Reading, MA, 1962), Chap. 2, pp. 64–103.

